www.springer.com/41230
https://doi.org/10.1007/s41230-022-2028-8

Effect of Ti, Sc and Zr additions on microstructure and mechanical properties of rheo-diecasting Al-6Zn-2Mg-2Cu alloys

Sai-heng Hou[1, 2, 3], *Jian Feng[1, 2, 3], Song Chen[1, 2, 3], Fan Zhang[1, 2, 3], and Da-quan Li[1, 2, 3]

1. State Key Laboratory of Nonferrous Metals and Processes, GRINM Group Co., Ltd., Beijing 100088, China

2. GRIMAT Engineering Institute Co., Ltd., Beijing 101407, China

3. General Research Institute for Nonferrous Metals, Beijing 100088, China

Abstract: The microstructure and mechanical properties of rheo-diecasting Al-6Zn-2Mg-2Cu alloys microalloyed with Ti, Sc and Sc+Zr were studied by optical microscopy (OM), scanning electron microscopy (SEM), X-ray diffraction (XRD), hardness testing, and tensile testing. The swirled equilibrium enthalpy device (SEED) process was introduced to prepare the semisolid slurry. Results show that the addition of Ti, Sc, and Sc+Zr refines the grain size and improves the uniformity of the semisolid slurry and then suppresses the growth of the α-Al grain during solution heat treatment. The microstructure of the four alloys in as-cast state mainly consists of spherical α-Al and the Mg(Al, Cu, Zn)$_2$ (η) eutectic phase. Moreover, primary Al_3Sc, Al_3(Sc, Zr) and Al_3Zr are also found in the micro-alloying alloys. After solution and aging heat treatment, most of the Mg(Al, Cu, Zn)$_2$ phases dissolve into the α-Al matrix, while part of Mg(Al, Cu, Zn)$_2$ phases transform to Al_2CuMg (S) phases. However, the coarse primary Al_3Sc and Al_3(Sc, Zr) still remain in the matrix, and promote crack initiation and propagation. With the tensile strength of 553 MPa, yield strength of 463 MPa and elongation of 13.4% at T6 state, trace Ti addition generates more attractive mechanical properties than the other three alloys.

Keywords: Al-Zn-Mg-Cu alloys; rheo-diecasting; microstructure; mechanical properties; micro-alloying

CLC numbers: TG146.21 **Document code:** A **Article ID:** 1672-6421(2023)02-125-09

1 Introduction

Al-Zn-Mg-Cu alloys (7xxx) belong to wrought aluminum alloys with high strength and toughness, which are widely used in aerospace and transportation fields [1, 2]. Al-Zn-Mg-Cu alloys are generally formed through wrought process, which is much more expensive than the alternative casting route. However, Al-Zn-Mg-Cu alloys prepared by traditional casting methods are prone to casting defects such as shrinkage porosity and shrinkage cavities, which will deteriorate the mechanical properties of the alloys [3, 4]. The semisolid metal processing technology discovered in 1971 provides the possibility for the direct casting of Al-Zn-Mg-Cu alloys [5]. This is because the semisolid metal processing technology has many advantages such as low casting temperature and small solidification shrinkage [6].

A very important method of strengthening Al-Zn-Mg-Cu alloys is to use certain elements for micro-alloying, which can make the alloy form a great number of nano-sized precipitates [7]. These precipitated phases can hinder the movement of dislocations, thereby increasing the strength of the alloys. Sc is a very good micro-alloying element in aluminum alloys, and can play a role in solid solution strengthening, precipitation strengthening and inhibiting recrystallization [8, 9]. Compared with other elements, the strengthening mechanism of Sc in Al is very unique [10, 11]. Although the solid solubility of Sc in Al is very low, it can increase strength while maintaining reasonable toughness. But, Sc is expensive, which limits its further application.

Adding small amounts of Sc+Zr to the aluminum alloys can reduce the cost. The addition of Zr can also modify the Sc-dispersoid by both refining its size and increasing its thermal stability [8, 12-15]. As such, the combined addition of Sc and Zr in aluminum alloys has a better strengthening effect by the precipitation of

***Jian Feng**

Ph. D, Engineer. His research interests focus on materials design for high performance casting aluminum alloys, including high strength and high toughness aluminum alloy, high thermal conductivity aluminum alloy, non-heat treatment aluminum alloy, and heat resistant aluminum alloy.

E-mail: fengjian@grinm.com

Received: 2022-03-08; Accepted: 2022-09-29

nano-scale Al_3Sc and $Al_3(Sc, Zr)$. In the semisolid forming of aluminum alloys, some studies have found that the addition of Sc or the combined addition of Sc and Zr can refine the semisolid slurry microstructure and the as-cast microstructure [16, 17]. However, owing to the unique process of semisolid slurry preparation and heat-treating for the semisolid alloys, the refinement and strengthening effects of Sc and Sc+Zr addition are uncertain. Moreover, in-depth analyses of the evolution of Sc-contained phase in the subsequent heat treatment process and its strengthening effect in semisolid forming are relatively few. Furthermore, as a commonly used refiner for traditional casting aluminum alloys, Al-5Ti-B master alloy is generally used to refine the α-Al phase, thus improving the mechanical properties [18, 19] and fluidity [20, 21] of the alloys. The refined microstructure of semisolid slurry is also beneficial to the subsequent die-casting, and can improve the mechanical properties of the alloys. Due to the higher cost of Sc and Zr in 7xxx series aluminum alloys, it is of great importance to compare the refining effect of Al-5Ti-B with Sc and Zr additions. Moreover, considering the unique solidification behavior, the research on the refining effect of Al-5Ti-B on semisolid die-casting is also very limited, especially on the semisolid slurry.

In order to reduce the cost of making high strength 7xxx series aluminum alloys and to accelerate its application in the automobile industry, the focus of this research is to compare the refining effect of Al-Ti-B with Sc and Zr additions in semisolid rheo-diecasting Al-6Zn-2Mg-2Cu alloys, especially on the microstructure of the semisolid slurry and the mechanical properties after heat treatment. In this study, the effects of trace Ti, Sc and Sc+Zr additions on the semisolid slurry, microstructure, and mechanical properties of semisolid rheo-diecasting Al-6Zn-2Mg-2Cu alloys were systematically studied.

2 Materials and methods

2.1 Alloy preparation and heat treatment

The experimental materials were prepared with pure Al, pure Zn, pure Mg, along with Al-50Cu, Al-2Sc, Al-5Zr, and Al-5Ti-B master alloys (all compositions are in wt.% unless otherwise noted). The Al-6Zn-2Mg-2Cu base alloy (7 alloy) modified with Ti, Sc and Sc+Zr was named 7T, 7S and 7SZ, respectively. The alloys were melted in a resistance furnace at 720 °C and degassed with argon using a rotary impeller. The melt was poured into a crucible with an inner diameter of 78 mm and a height of 210 mm at 650 °C. The semisolid slurry was prepared by the swirled equilibrium enthalpy device (SEED) process at an eccentric rotation (swirling) speed of 180 rpm. Subsequently, the prepared semisolid slurry was transferred to the Buhler 340-ton die-casting machine with a boost pressure of 95 MPa and a filling speed of 0.2 $m \cdot s^{-1}$ to fabricate the as-cast samples of the studied alloy. The actual chemical composition of the studied alloys was analyzed by ICP-AES, and the results are shown in Table 1. The liquidus and solidus temperatures of the studied alloys were calculated by JMatPro software, and found to be 631 °C and 451 °C, respectively. According to the DSC curve analysis in Ref. [22], the beginning temperature of $Mg(Al, Cu, Zn)_2$ phase dissolved into α-Al is about 480 °C. The solution temperature of Al-Zn-Mg-Cu alloys is usually 470–475 °C [22, 23]. Therefore, the as-cast samples were solution heat treated at 470 °C for 8 h, and then aged at 120 °C for different times.

2.2 Microstructure observation

For the semisolid slurry microstructure analysis, the slurry was rapidly quenched into cold water to obtain the as-quenched slurry, and the samples for optical microscopy (OM) analysis were sectioned horizontally from the middle of the as-quenched slurry, as displayed in Fig. 1(a). For the as-cast sample analysis of the studied alloys after high pressure die-casting, the sampling location is shown in Fig. 1(b). The samples were etched with Keller's reagent (5 mL HF, 10 mL HNO_3, and 85 mL H_2O) after mechanical polishing. The grain size and shape factor of the semisolid slurry were analyzed by image processing and analysis software (Image-Pro Plus 6.0 software). The grain size of primary α-Al was calculated by the method of section line, and the shape factor (F) was calculated by $F=4\pi A/P^2$ (where A represents the area of a grain, and P represents the perimeter of a grain). The microstructure observation of the as-cast samples in Fig. 1(b) and local chemical analysis were carried out using a scanning electron microscope (SEM) equipped with energy dispersive spectroscopy (EDS) apparatus. The phase analysis was carried out by X-ray diffraction (XRD) with a scanning speed of $8° \cdot min^{-1}$ and 2θ angle between 10° and 90°.

2.3 Mechanical property testing

Tensile testing was performed on a universal testing machine of E45.305 (MTS Systems Co., Ltd.), and a schematic of the tensile specimen is shown in Fig. 2. The microhardness was measured by a Vickers-hardness tester under a load of 5 kg for 15 s. For each composition alloy, 5 tests were performed and the average value was calculated.

Table 1: Actual compositions of studied alloys (wt.%)

Alloys	Zn	Mg	Cu	Ti	Sc	Zr	Fe	Si	Al
7 alloy	6.43	2.28	2.29				0.007	<0.0003	Bal.
7T alloy	5.98	2.28	2.04	0.15			<0.0001	0.017	Bal.
7S alloy	5.86	2.02	1.79		0.42		0.03	0.008	Bal.
7SZ alloy	6.06	1.99	1.90		0.17	0.14	0.03	0.008	Bal.

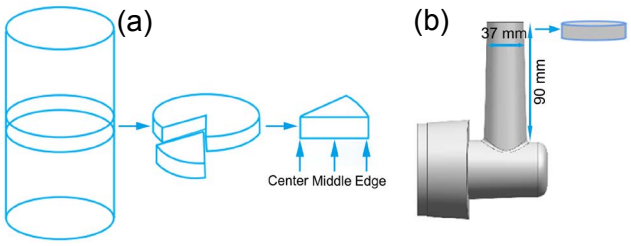

Fig. 1: Schematics of sampling of semisolid slurry (a) and as-cast state (b)

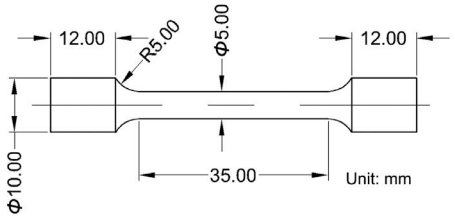

Fig. 2: Schematics of tensile specimen

3 Results

3.1 Microstructure of semisolid slurries

Figure 3 shows the semisolid slurry microstructure of the four experimental alloys. The statistical results of the average grain size and shape factor for different areas are shown in Fig. 4. It can be seen that adding a small amount of Ti, Sc or Sc+Zr to the alloy can refine the α-Al grains and increase its shape factor. There are coarse primary α-Al dendrites in various positions of the slurry of the Al-6Zn-2Mg-2Cu alloy (7 alloy) without adding trace elements. The average α-Al diameters at different locations of the 7 alloy from the edge to the center are 173 μm, 174 μm and 186 μm, respectively. Firstly, the middle area was selected to show the refinement of Ti, Sc and Sc+Zr additions [Fig. 4(a)]. The average α-Al grain size dramatically reduces from 174 μm of the 7 alloy to 112 μm of the 7T alloy, 94 μm of the 7S alloy and 120 μm of the 7SZ

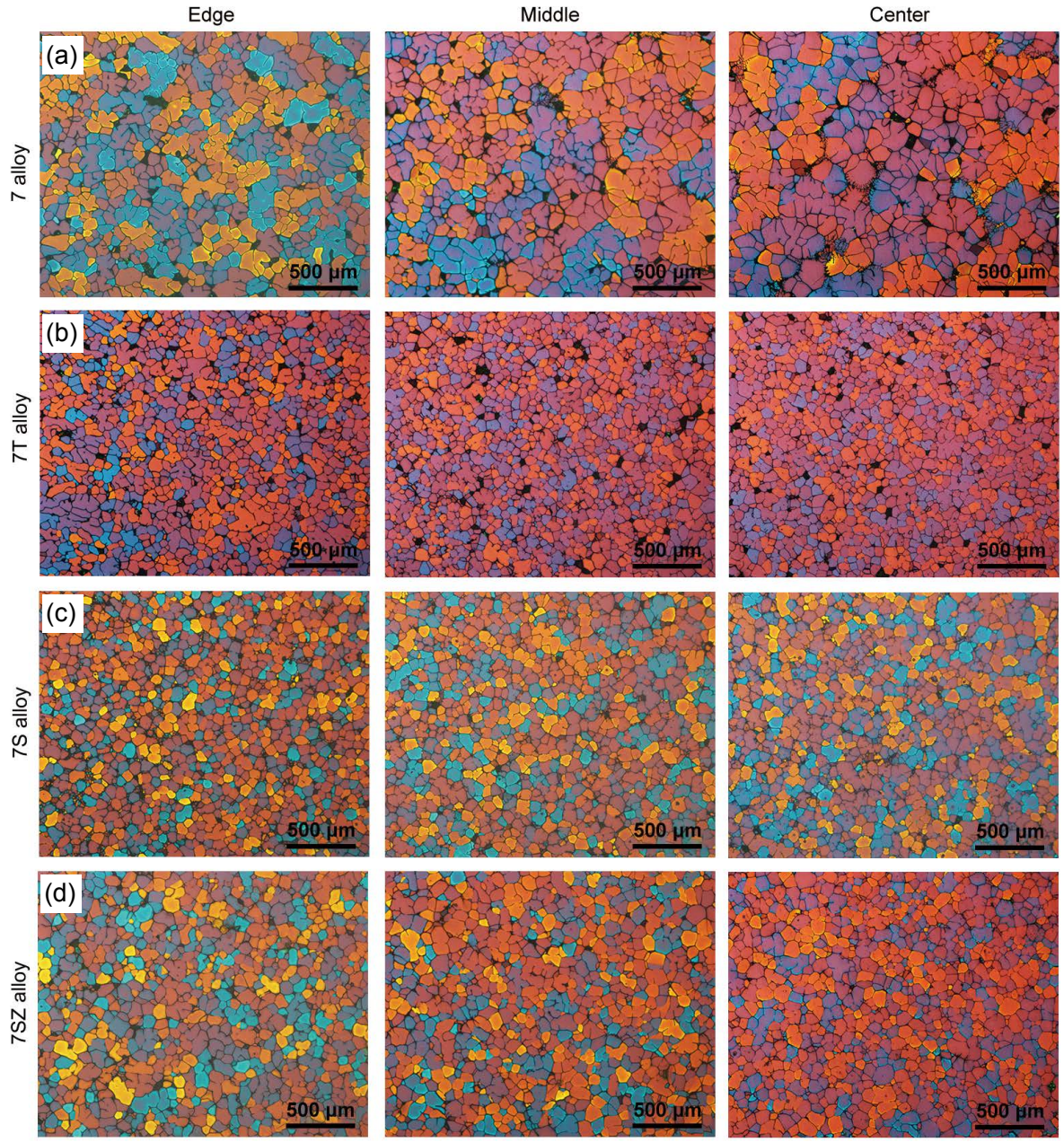

Fig. 3: Microstructures of semisolid slurry in different alloys: (a) 7; (b) 7T; (c) 7S; (d) 7SZ

alloy, respectively. Secondly, the homogeneity of the semisolid slurry from edge area to center area is also improved. The standard deviation (STDEV) of the average grain size for three positions was introduced to evaluate the homogeneity. The STDEV value for the 7 alloy is 7.23. After adding a small amount of Ti, Sc or Sc+Zr to the 7 alloy, the STDEV value decreases to 1.73 of the 7T alloy, 2.00 of the 7S alloy and 4.16 of the 7SZ alloy. The lower STDEV value indicates that the addition of Ti, Sc and Sc+Zr enhances the homogeneity of the semisolid slurry. In other words, the microstructure of the semisolid slurry is significantly refined and homogenized after adding trace Ti, Sc and Sc+Zr.

Figure 4(b) indicates that the average shape factor, the roundness of the primary α-Al is also affected by the addition of trace elements Ti, Sc and Sc+Zr. The average shape factor of three different areas of the primary α-Al grains is 0.35 for 7 alloy, and 0.55 for 7T, which is higher than that of the 7 alloy. Adding Sc and Sc+Zr to the 7 alloy, the average shape factor of 7S and 7SZ alloy both increases to 0.68 and 0.65, respectively. Moreover, the average shape factor slowly increases from the edge to center of the four studied alloys. For example, the shape factor of 7T alloy increases from 0.44 of the edge area to 0.58 of the center area. Combining the results in Fig. 4(a) and Fig. 4(b), it is concluded that the addition of Ti, Sc and Sc+Zr refines the α-Al grain size, improves the homogeneity and promotes the formation of spherical structure of the semisolid slurry.

3.2 Microstructure of as-cast and as-solution alloy

The microstructure and the statistical results of grain size of the alloys in different states are shown in Fig. 5 and Fig. 6, respectively. The average grain size of the 7 alloy in as-cast is 85 μm, while the average grain sizes of the alloy with a small amount of Ti, Sc and Sc+Zr are 72 μm, 68 μm and 74 μm, respectively. That is to say, a slightly refinement of α-Al grain is observed in as-cast state. After solution heat treatment, the average grain size of 7 alloy increases to about 286 μm, while the alloys containing Ti, Sc and Sc+Zr slowly increase to 88 μm, 87 μm and 91 μm, respectively. It's clearly shown that the grain size of the 7 alloy increases by 201 μm after solution heat treatment, while the grain size of 7T, 7S and 7SZ alloys only increases by 16 μm, 19 μm and 17 μm, respectively. Therefore, the addition of Ti, Sc and Sc+Zr to Al-6Zn-2Mg-2Cu alloy strongly inhibits the grain growth during solution heat treatment.

Figure 7 shows the XRD patterns of as-cast and as-solution alloys. It can be seen from the diffraction peaks in the as-cast samples that the intermetallic phases present in the four alloys are mainly $Mg(Al, Cu, Zn)_2$ phase. As the atomic size of Al and Cu are similar with Zn, they can easily replace the Zn atoms in the $MgZn_2$ phase to form the $Mg(Al, Cu, Zn)_2$ phase. In addition to the diffraction peaks of $Mg(Al, Cu, Zn)_2$, the Al_3Sc and Al_3Zr phases are also detected in 7S and 7SZ alloys.

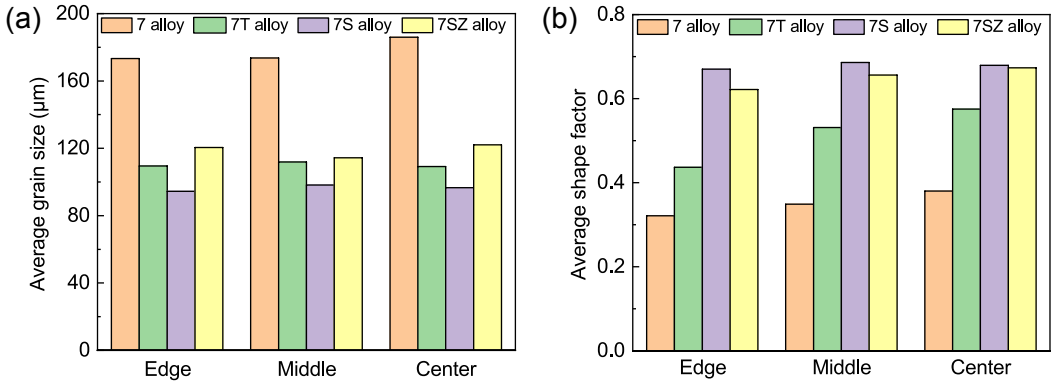

Fig. 4: Statistical results for average grain size (a) and average shape factor (b) of semisolid slurry of different alloys

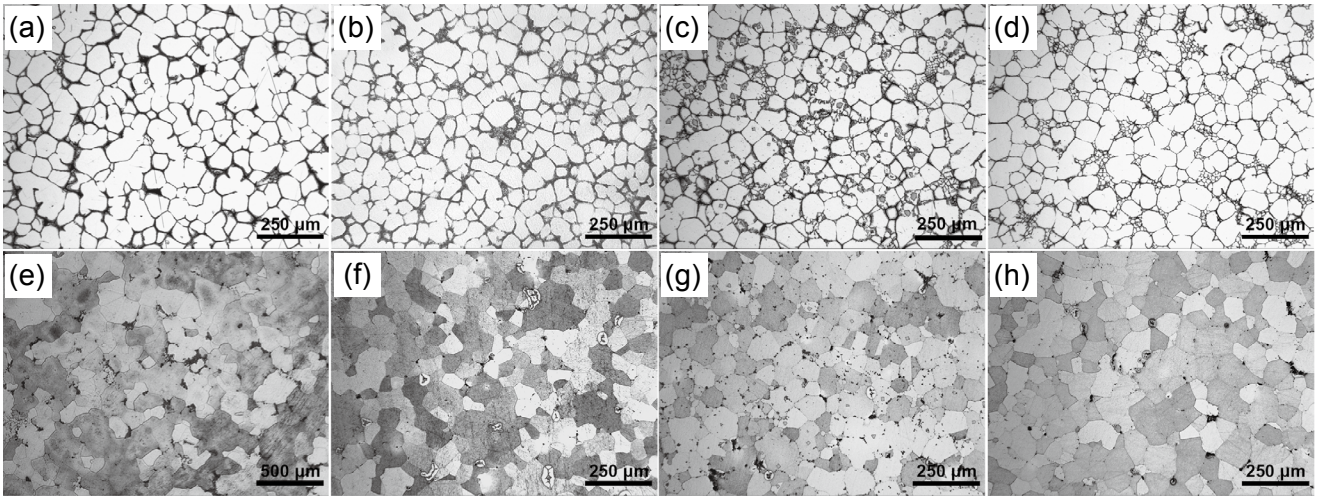

Fig. 5: Microstructures of as-cast (a–d) and as-solution (e–h) alloys: (a, e) 7 alloy; (b, f) 7T alloy; (c, g) 7S alloy; (d, h) 7SZ alloy

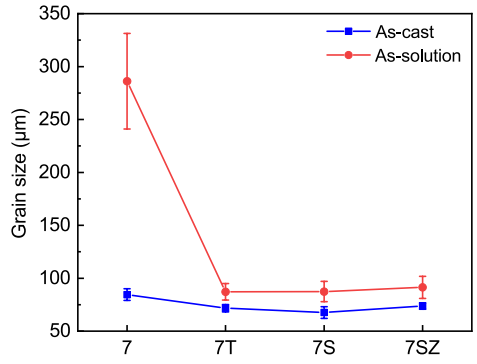

Fig. 6: Statistical results for grain size of as-cast and as-solution alloys

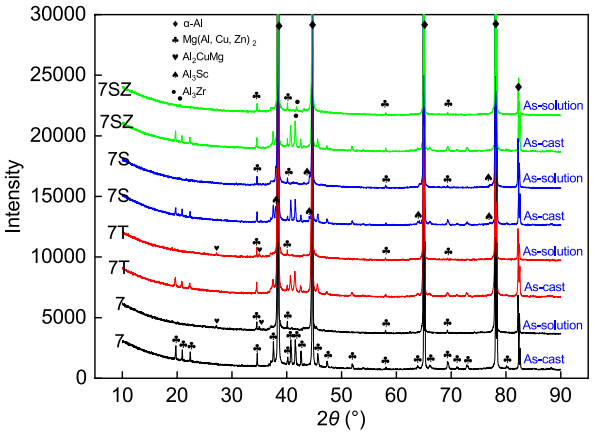

Fig. 7: XRD diffraction patterns of as-cast and as-solution alloys with identified phases

However, the diffraction peak of Al_3Ti phase is not found in 7T alloy. This is probably due to the relatively small content of primary Al_3Ti phase. After solution heat treatment, most of the $Mg(Al, Cu, Zn)_2$ phases dissolve into the α-Al matrix, as suggested by the difference of the diffraction peaks of the $Mg(Al, Cu, Zn)_2$ phase. Moreover, the diffraction peaks of new Al_2CuMg phase appear in heat treated 7 alloy and 7T alloy, indicating that new Al_2CuMg phase is formed during heat treatment. The diffraction peaks of primary Al_3Sc and Al_3Zr do not change before and after heat treatment, indicating that they cannot dissolve into the α-Al matrix during heat treatment.

In order to characterize the microstructure of the as-cast and as-solution alloys, SEM observation was performed, and the results are shown in Fig. 8. The corresponding EDS results of the phases in Fig. 8 are also listed in Table 2. As shown in Fig. 8(a), abundant eutectic structure is observed in the grain boundary of the as-cast 7 alloy, and the EDS result of Point 1 confirms that this phase is $Mg(Al, Cu, Zn)_2$. The addition of Ti, Sc and Sc+Zr promotes the formation of Al_3Ti (Point 2), Al_3Sc (Point 4) and $Al_3(Sc, Zr)$ phases (Points 6 and 8) shown in Figs. 8(b–e), respectively. Moreover, the primary Al_3Ti, Al_3Sc, and $Al_3(Sc, Zr)$ phases precipitate in α-Al grains, indicating that these phases can act as heterogeneous nuclei, promote the nucleation of α-Al, and thus refine the microstructure of the as-cast alloys. Combining the XRD results of the studied as-cast alloys in Fig. 7, it is concluded that the as-cast microstructure mainly consists of α-Al and $Mg(Al, Cu, Zn)_2$ phase. The addition of Sc and Sc+Zr leads to coarse primary Al_3Sc and $Al_3(Sc, Zr)$

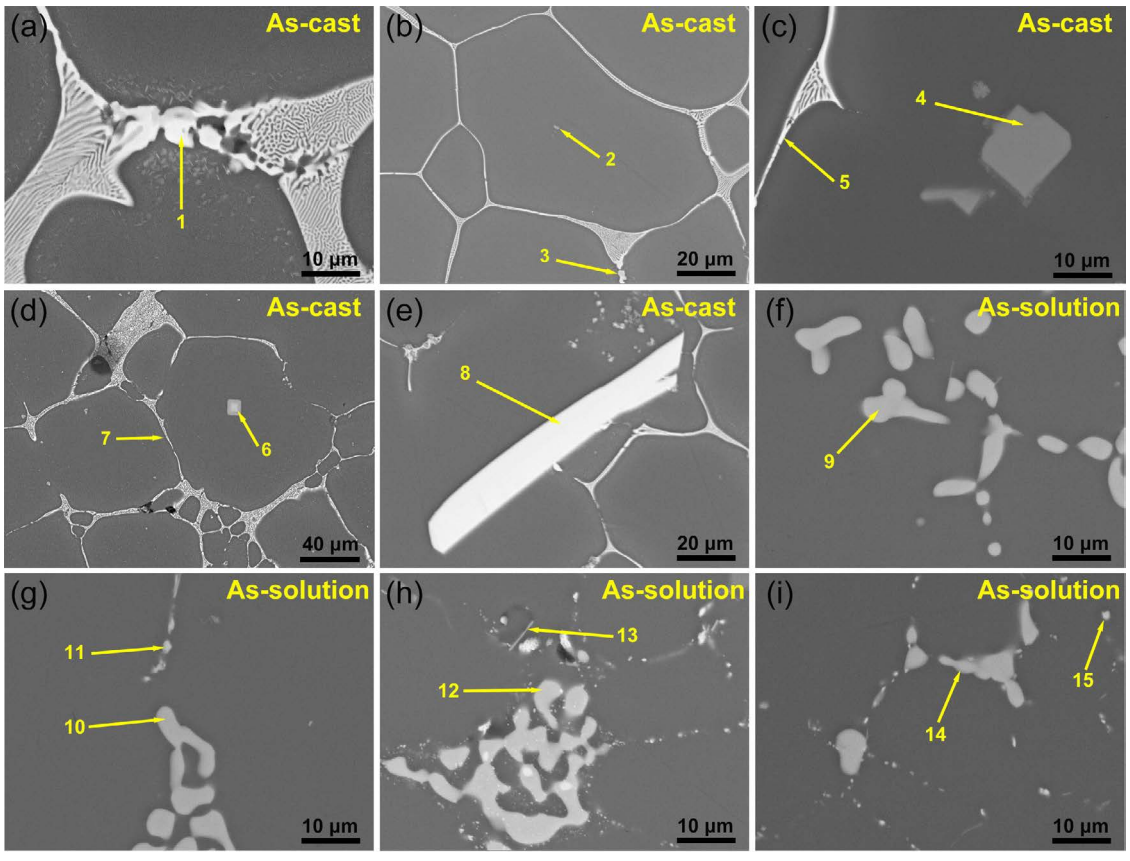

Fig. 8: Representative backscattered SEM images of as-cast (a–e) and as-solution (f–i) alloys: (a, f) 7 alloy; (b, g) 7T alloy; (c, h) 7S alloy; (d, e, i) 7SZ alloy

Table 2: EDS results of selected constituent particles highlighted in Fig. 8 (at.%)

Point	Al	Zn	Mg	Cu	Fe	Ti	Sc	Zr	Closest phase
1	24.94	32.15	31.45	11.46					$Mg(Al, Cu, Zn)_2$
2	69.61		2.82			27.57			Al_3Ti
3	41.36	20.04	25.74	12.86					$Mg(Al, Cu, Zn)_2$
4	74.97	0.94					24.09		Al_3Sc
5	65.99	10.68	15.56	7.78					$Mg(Al, Cu, Zn)_2$
6	84.90						7.10	7.99	$Al_3(Sc, Zr)$
7	61.93	15.98	17.98	4.11					$Mg(Al, Cu, Zn)_2$
8	78.70						4.60	16.70	$Al_3(Sc, Zr)$
9	56.89	1.88	22.98	18.16					Al_2CuMg
10	59.35	1.42	21.30	17.93					Al_2CuMg
11	84.43	0.93	2.91	8.09	3.63				Al_7Cu_2Fe
12	57.63	1.46	22.34	18.56					Al_2CuMg
13	90.77	1.77	3.36	2.97	1.13				Al_7Cu_2Fe
14	61.38	1.63	21.23	15.77					Al_2CuMg
15	86.50	0.91	3.05	6.37	3.16				Al_7Cu_2Fe

phase in α-Al grain. However, trace Ti addition only forms fine and small point-like precipitates. Considering the lower Ti content, this is the reason that the diffraction peaks of Al_3Ti phase were not detected in Fig. 7.

Figures 8(f–i) show higher magnification images of eutectic zone of the studied alloys after solution treatment. The EDS results in Table 2 show the existence of coarse Al_2CuMg phase (Points 9, 10, 12, and 14). These results clearly identify the transformation from $Mg(Al, Cu, Zn)_2$ phase to Al_2CuMg phase during solution treatment for the studied alloys. This is because of the higher solid solubility and diffusion rate of Zn and Mg elements in α-Al matrix. Furthermore, small point-like (Points 11 and 15) and short rod-like (Point 13) Al_7Cu_2Fe phases are also observed. As a lower Fe content (<0.1%) in the four studied alloys, this phase does not coarsen. Furthermore, the content of Al_7Cu_2Fe phase is almost the same in the four alloys after heat treatment and is very low. Thus, the effect of this phase on the mechanical properties of the studied alloys is negligible.

3.3 Mechanical properties

Figure 9 shows the variation of the hardness of the four alloys after solution treatment at 470 °C for 8 h and then artificial aging at 120 °C for varying times, displaying the characteristic of age-hardening behavior. The as-solution hardness is shown as the first data point on each curve. It can be observed that the hardness increases rapidly with prolonged time before 24 h, and further increasing the time to 48 h, no obvious

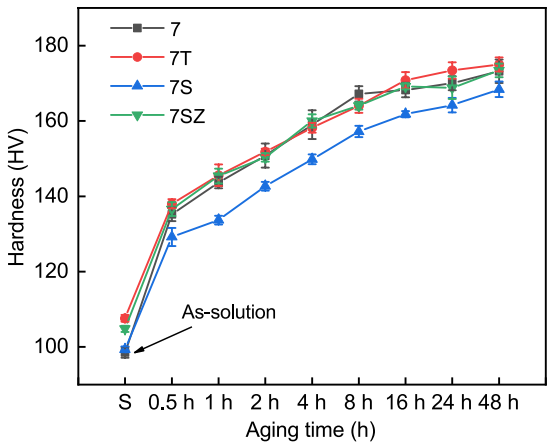

Fig. 9: Hardening curves of four alloys treated by artificial aging at 120 °C

enhancement is observed. Therefore, the aging time at 24 h was chosen as an optimized parameter to investigate the tensile properties of the four alloys.

Figure 10 illustrates the tensile properties of the studied alloys after solution treatment at 470 °C for 8 h and artificial aging at 120 °C for 24 h. It can be seen that the average ultimate tensile strength (UTS) and yield strength (YS) of the four alloys are similar. The average elongation (EL) of 7T alloys (13.4%) is much higher than that of 7 alloys (10.6%). It is worth noting that the EL of 7S and 7SZ alloys is decreased to about 7%. Therefore, 7T alloy has the best comprehensive mechanical properties.

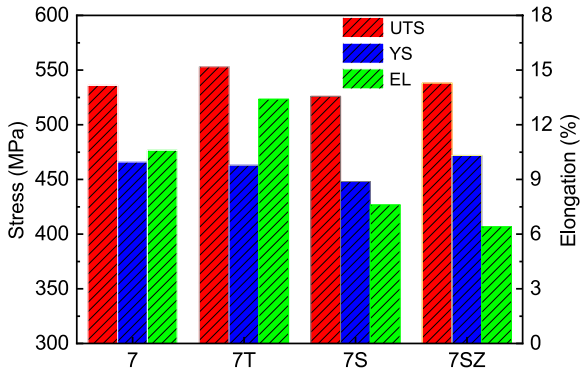

Fig. 10: Mechanical properties of four alloys in T6 state (470 °C-8 h+120 °C-24 h)

4 Discussion

4.1 Microstructure

According to the phase diagram in Fig. 11(a), the formation of primary Al_3Sc requires that the binary Al-Sc alloy is hypereutectic with respect to Sc, i.e., in excess of approximately 0.6wt.% [24]. However, in Al-Zn-Mg-Cu alloys, the addition of 0.2wt.%–0.3wt.% Sc is enough to form the Al_3Sc phase and refine the grains effectively [25]. In this study, the addition of Sc content in 7S alloys is up to 0.4wt.% (less than eutectic composition at approximately 0.6wt.%), which is higher than that in Ref. [25]. Therefore, it is easy to form primary Al_3Sc phase. According to the binary phase diagram of Al-Zr in Fig. 11(b), the formation of primary Al_3Zr is similar to that of primary Al_3Sc [26]. The formation of primary $Al_3(Sc, Zr)$ in Al-Zn-Mg-Cu alloys containing Sc and Zr has been studied in Ref. [27]. Most primary $Al_3(Sc,Zr)$ phases have a cubic three-dimensional morphology. The morphology of Point 8 in Fig. 8(e) is the same as that of primary $Al_3(Sc, Zr)$. Primary $Al_3(Sc, Zr)$ is also detected in 7SZ alloys. The addition of a small amount of Ti in Al alloys can well refine the α-Al grain size [18, 19]. According to the lattice parameter analysis in Table 3 [28], the primary Al_3Ti, Al_3Sc and $Al_3(Sc, Zr)$ phases can act as effective heterogeneous nucleation sites, and then refine the α-Al grains. Over all, the addition of Ti, Sc and Sc+Zr refines the α-Al grains of the studied alloys.

The Sc and Zr added in the alloys are basically used to form the primary phases, and their supersaturation in α-Al is very low. Lohar et al. [29] studied the influence of cooling rate on the microstructure and aging behavior of as-cast Al-Sc-Zr alloy. When the cooling rate was 0.16 °C·s^{-1}, Sc and Zr mainly formed coarse primary phases, while the supersaturated Sc and Zr in α-Al was very low, and the subsequent strengthening effect was not obvious. Only when the cooling rate increases to 7.69 °C·s^{-1}, can it play a very good strengthening effect. The lower cooling rate in semisolid slurry preparation leads to the formation of coarse primary Al_3Sc and $Al_3(Sc, Zr)$ phase, indicating that the subsequent strengthening effect is not obvious. Based on the analysis in Fig. 8, the $Mg(Al, Cu, Zn)_2$ phases in as-cast alloys are not affected by the addition of trace elements Ti, Sc and Sc+Zr. Since the diffusion rate of Zn and Mg atoms in α-Al is greater than that of Cu atoms, some of the $Mg(Al, Cu, Zn)_2$ phases are transformed into Al_2CuMg phase after solution heat treatment [Figs. 8(f–i)]. Based on the XRD patterns in Fig. 7, the primary Al_3Sc and $Al_3(Sc, Zr)$ phases cannot dissolve into α-Al matrix. As a result, in semisolid rheo-diecasting Al-Zn-Mg-Cu alloy, adding a small amount of Ti, Sc and Sc+Zr has similar effect of refining α-Al, while the Ti contained alloy does not form a coarse primary phase [primary Al_3Sc and $Al_3(Sc, Zr)$].

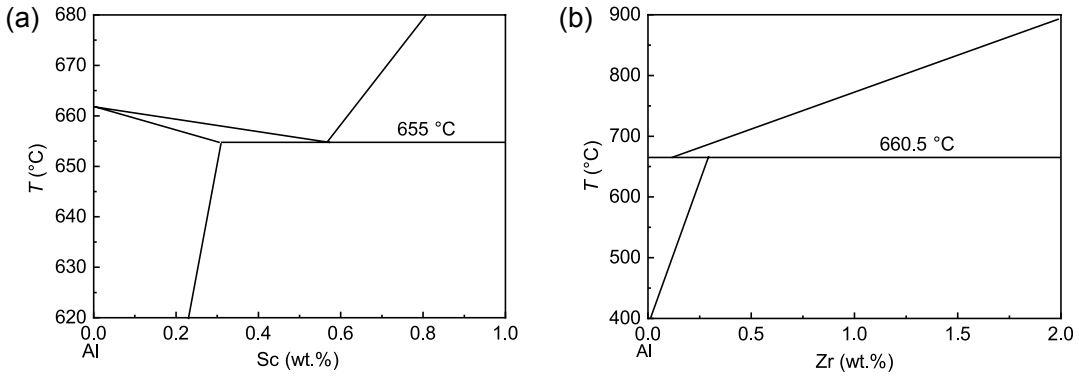

Fig. 11: Part of Al-Sc phase diagram adapted from Ref. [24] (a) and Al-Zr phase diagram adapted from Ref. [26] (b)

Table 3: Lattice parameters and corresponding mismatch with α-Al for cubic ($L1_2$) and related tetragonal ($D0_{22}$ or $D0_{23}$) Al_3M trialuminide intermetallic compounds

Phase	Structure	Lattice parameters (Å)	Mismatch with Al	Absolute mismatch, δ	Ref.
Al_3Ti	$L1_2$	*a*=3.967	–2.04%	2.04%	[28]
	$D0_{22}$	*a*=3.848	–4.98%	5.36%	[28]
		c=8.596	+6.13%		
Al_3Sc	$L1_2$	*a*=4.103	+1.32%	1.32%	[28]

4.2 Mechanical properties

The hardness of the four alloys gradually increases during the artificial aging at 120 °C, as shown in Fig. 9. This is mainly attributed to the gradual precipitation of η' ($MgZn_2$) phase in the α-Al matrix, which can effectively hinder the movement of dislocations, and then enhance the mechanical properties [30-32]. As can be seen in Fig. 10, no obvious improvement of the UTS and YS of the four alloys was observed. The solidification of 7S and 7SZ alloys forms the primary Al_3Sc and $Al_3(Sc, Zr)$ phase, which consumes a large amount of Sc and Zr atoms, resulting in lower supersaturation of Sc and Zr in the α-Al matrix, and almost no nanoscale Al_3Sc and $Al_3(Sc_{1-x}Zr_x)$ precipitates during heat treatment. Therefore, the precipitation of η' ($MgZn_2$) phase from the α-Al matrix during the artificial aging process will not be affected. The close hardness values of the four alloys reflected in Fig. 9 can also explain this phenomenon. The strength of aluminum alloys can be improved by refining the grain size, and the strengthening effect is given by Refs. [33, 34]:

$$\sigma_s = \sigma_0 + kd^{-1/2} \quad (1)$$

where σ_s is the yield strength, σ_0 is a constant, k is about 68 MPa·μm$^{1/2}$ for aluminum alloy, d is the average grain size.

Considering the lower aging temperature of 120 °C has little effect on the grain size, the microstructure in as-solution state is used to investigate the refining effect of Ti, Sc and Sc+Zr addition rather than solution and aging state. As shown in Fig. 6, the addition of Ti, Sc and Sc+Zr reduces the grain size from 286 μm of the 7 alloy to 88 μm, 87 μm and 91 μm after solution heat treatment, respectively. Calculated from Eq. (1), the strength increment is 3.2 MPa of 7T alloy, 3.3 MPa of 7S alloy and 3.1 MPa of 7SZ alloy. In other words, the effect of the grain refining of the alloys on the strength increment is not significant. Therefore, the main strengthening effect of all the alloys in this study is primarily achieved by the precipitation of nano-scale η' ($MgZn_2$) phases. Moreover, the hardness variation of the studied alloys in Fig. 9 also confirms that the addition of minor Ti, Sc and Sc+Zr generates little extra precipitation strengthening effect by nano-scale Al_3Sc and $Al_3(Sc, Zr)$ phase. As a result, the strength of the four alloys is very close, as shown in Fig. 10. The process of preparing semisolid slurry is at 650 °C for 100 s, which is lower than the precipitation temperature of Al_3Sc and Al_3Zr (as shown in Fig. 11). The cooling rate of the melt is very slow in this process, only about 0.1 °C·s^{-1}. The lower cooling rate results in the small degree of undercooling, so that the nucleation rate of the primary phases [primary Al_3Sc, $Al_3(Sc, Zr)$ and Al_3Zr] is low. In addition, the swirling of the crucible during the preparation of the semisolid slurry makes the temperature and composition of the melt more uniform, which promotes the gradual growth of the nucleated primary phases. Finally, the firstly solidified primary Al_3Sc and Al_3Zr are easily coarsened during the preparation of semisolid slurry, while in the later heat treatment process, they have excellent thermal stability and generate little strengthening effect by the precipitation of nano-scale Al_3Sc and $Al_3(Sc, Zr)$ phase. Furthermore, because of the presence of coarse primary Al_3Sc and $Al_3(Sc, Zr)$ phase (as shown in Fig. 8), it is easy to cause stress concentration and microcracks at the interface between primary phases and α-Al in the tensile experiment, so the elongation of 7S and 7SZ alloys decreases sharply. The morphology of Al_3Ti phase is fine and small point-like in 7T alloy [Fig. 8(b)]. That is to say, no coarse primary Al_3Ti phase is formed, and then the crack is not easy to initiation and propagation. Therefore, the 7T alloy possesses higher elongation than the 7S and 7SZ alloys.

5 Conclusions

(1) The average α-Al diameters of the semisolid slurry of the Al-6Zn-2Mg-2Cu alloy from the edge to the center are 173 μm, 174 μm, 186 μm, respectively. The addition of Ti, Sc and Sc+Zr refines the α-Al grain size, improves the homogeneity and promotes the formation of spherical structure of the semisolid slurry.

(2) The average α-Al grain size of the as-cast 7 alloy is 85 μm, while the average grain sizes of the alloy with a small amount of Ti, Sc and Sc+Zr are 72 μm, 68 μm and 74 μm, respectively. After solution heat treatment, the average grain size of the 7 alloy increases to 286 μm, while the grain size of 7T, 7S and 7SZ alloys slowly increases to 88 μm, 87 μm and 91 μm, respectively. It is clearly shown that the addition of Ti, Sc and Sc+Zr to Al-6Zn-2Mg-2Cu alloy strongly inhibits the grain growth during solution heat treatment.

(3) The eutectic phases of the four as-cast alloys are mainly $Mg(Al, Cu, Zn)_2$ phase. The addition of Sc and Sc+Zr leads to the formation of coarse primary Al_3Sc and $Al_3(Sc, Zr)$ phase in α-Al grains, while the Ti addition only forms small Al_3Ti phase. After solution heat treatment, most of the $Mg(Al, Cu, Zn)_2$ phases dissolve into α-Al matrix, and a new Al_2CuMg phase is formed.

(4) The refinement of alloy microstructure by adding trace Ti, Sc and Sc+Zr does not contribute much to the strength of the aluminum alloy. The elongation of 7S and 7SZ alloys is about 35% lower than that of 7 alloy, while the elongation of 7T alloy reaches 13.4%, which is 26% higher than that of the 7 alloy. With the tensile strength of 553 MPa and yield strength of 463 MPa, the comprehensive mechanical properties of the 7T alloy are the best.

Acknowledgement

The authors would like to express gratitude for the financial support from the National Key R&D Program of China (No. 2016YFB0301003).

Conflict of interest

The authors declare that they have no conflict of interest.

References

[1] Williams J C, Starke Jr. Progress in structural materials for aerospace systems. Acta Materialia, 2003, 51(19): 5775–5799.
[2] Huda Z, Edi P. Materials selection in design of structures and engines of supersonic aircrafts: A review. Materials & Design, 2013, 46: 552–560.
[3] Thanabumrungkul S, Janudom S, Burapa R, et al. Industrial development of gas induced semisolid process. Transactions of Nonferrous Metals Society of China, 2010, 20: 1016–1021.
[4] Kim S, Kim D, Kim W, et al. The study on characteristics of heat treatment of the direct squeeze cast 7075 wrought Al alloy. Materials Science and Engineering: A, 2001, 304: 721–726.
[5] Spencer D, Mehrabian R, Flemings M C, et al. Rheological behavior of Sn-15 pct Pb in the crystallization range. Metallurgical and Materials Transactions B, 1972, 3(7): 1925–1932.
[6] Atkinson H V. Modelling the semisolid processing of metallic alloys. Progress in Materials Science, 2005, 50(3): 341–412.
[7] Gladman T. Precipitation hardening in metals. Materials Science and Technology, 1999, 15(1): 30–36.
[8] Toropova L S, Eskin D G, Kharakterova M L, et al. Advanced aluminum alloys containing scandium: Structure and properties. Gondon and Breach Science, 1998, 115.
[9] Kendig K L, Miracle D B. Strengthening mechanisms of an Al-Mg-Sc-Zr alloy. Acta Materialia, 2002, 50(16): 4165–4175.
[10] Marquis E A, Seidman D N. Nanoscale structural evolution of Al_3Sc precipitates in Al(Sc) alloys. Acta Materialia, 2001, 49(11): 1909–1919.
[11] Marquis E A, Seidman D N, Dunand D C. Effect of Mg addition on the creep and yield behavior of an Al-Sc alloy. Acta Materialia, 2003, 51(16): 4751–4760.
[12] Fuller C B, Seidman D N, Dunand D C. Mechanical properties of Al(Sc, Zr) alloys at ambient and elevated temperatures. Acta Materialia, 2003, 51(16): 4803–4814.
[13] Davydov V, Rostova T, Zakharov V, et al. Scientific principles of making an alloying addition of scandium to aluminium alloys. Materials Science and Engineering: A, 2000, 280(1): 30–36.
[14] Robson J D. A new model for prediction of dispersoid precipitation in aluminium alloys containing zirconium and scandium. Acta Materialia, 2004, 52(6): 1409–1421.
[15] Knipling K E, Seidman D N, Dunand D C. Ambient- and high-temperature mechanical properties of isochronally aged Al-0.06Sc, Al-0.06Zr and Al-0.06Sc-0.06Zr (at.%) alloys. Acta Materialia, 2011, 59(3): 943–954.
[16] Zhao J W, Guo A, Li H, et al. Semisolid slurry of 7A04 aluminum alloy prepared by electromagnetic stirring and Sc, Zr additions. China Foundry, 2017, 14(3): 188–193.
[17] Zhao J, Xu C, Dai G, et al. Microstructure and properties of rheo-diecasting wrought aluminum alloy with Sc additions. Materials Letters, 2016, 173: 22–25.
[18] Cook R, Cooper P, Kearns M. Benefits of master alloy melt treatments in the aluminum foundry industry. Minerals, Metals and Materials Society, Warrendale, PA (United States), 1996.
[19] Apelian D, Sigworth G K, Whaler K R. Assessment of grain refinement and modification of Al-Si foundry alloys by thermal analysis. AFS Trans., 1984, 92(2): 297–307.
[20] Mollard F R, Flemings M C, Niyama E F. Aluminum fluidity in casting. JOM, 1987, 39: 34–37.
[21] Dahle A, Tøndel P, Paradies C, et al. Effect of grain refinement on the fluidity of two commercial Al-Si foundry alloys. Metallurgical and Materials Transactions A, 1996, 27(8): 2305–2313.
[22] Ditta A, Wei L, Xu Y, et al. Effect of hot extrusion and optimal solution treatment on microstructure and properties of spray-formed Al-11.3Zn-2.65Mg-1Cu alloy. Journal of Alloys and Compounds, 2019, 797: 558–565.
[23] Ghosh A, Ghosh M, Kalsar R. Influence of homogenisation time on evolution of eutectic phases, dispersoid behaviour and crystallographic texture for Al-Zn-Mg-Cu-Ag alloy. Journal of Alloys and Compounds, 2019, 802: 276–289.
[24] Norman A F, Prangnell P B, McEwen R S. The solidification behaviour of dilute aluminium-scandium alloys. Acta Materialia, 1998, 46(16): 5715–5732.
[25] Mousavi M G, Cross C E, Grong Ø. Effect of scandium and titanium-boron on grain refinement and hot cracking of aluminium alloy 7108. Science and Technology of Welding and Joining, 1999, 4(6): 381–388.
[26] Okamoto H. Al-Zr (aluminum-zirconium). Journal of Phase Equilibria and Diffusion, 2002, 23(5): 455.
[27] Li J H, Wiessner M, Albu M, et al. Correlative characterization of primary Al_3(Sc, Zr) phase in an Al-Zn-Mg based alloy. Materials Characterization, 2015, 102: 62–70.
[28] Knipling K E, Dunand D C, Seidman D N. Criteria for developing castable, creep-resistant aluminum-based alloys – A review. International Journal of Materials Research, 2006, 97(3): 246–265.
[29] Lohar A K, Mondal B N, Panigrahi S C. Influence of cooling rate on the microstructure and ageing behavior of as-cast Al-Sc-Zr alloy. Journal of Materials Processing Technology, 2010, 210(15): 2135–2141.
[30] Dumont D, Deschamps A, Bréchet Y, et al. Characterisation of precipitation microstructures in aluminium alloys 7040 and 7050 and their relationship to mechanical behaviour. Materials Science and Technology, 2004, 20(5): 567–576.
[31] Fan X G, Jiang D M, Meng Q C, et al. Characterization of precipitation microstructure and properties of 7150 aluminium alloy. Materials Science and Engineering: A, 2006, 427(1–2): 130–135.
[32] Zhang M, Liu T, He C N, et al. Evolution of microstructure and properties of Al-Zn-Mg-Cu-Sc-Zr alloy during aging treatment. Journal of Alloys and Compounds, 2016, 658: 946–951.
[33] Yu H H, Xin Y C, Wang M Y, et al. Hall-Petch relationship in Mg alloys: A review. Journal of Materials Science & Technology, 2018, 34(2): 248–256.
[34] Shanmugasundaram T, Heilmaier M, Murty B S, et al. On the Hall-Petch relationship in a nanostructured Al-Cu alloy. Materials Science and Engineering: A, 2010, 527(29–30): 7821–7825.